Environmental Science & Technology

Article

pubs.acs.org/est

Size-Controlled Dissolution of Organic-Coated Silver Nanoparticles

Rui Ma,[†,‡] Clément Levard,[†,∥] Stella M. Marinakos,[†] Yingwen Cheng,[†,§] Jie Liu,[†,§] F. Marc Michel,[†,∥,⊥] Gordon E. Brown, Jr.,[†,∥,⊥,#] and Gregory V. Lowry*[,†,‡]

[†]Center for the Environmental Implications of NanoTechnology (CEINT), Duke University, Durham, North Carolina 27708,
[‡]Department of Civil & Environmental Engineering, Carnegie Mellon University, Pittsburgh, Pennsylvania 15213,
[§]Department of Chemistry, Duke University, Durham, NC27708,
[∥]Department of Geological & Environmental Sciences, Stanford University, Stanford, California 94305, United States
[⊥]Stanford Synchrotron Radiation Lightsource, SLAC National Accelerator Laboratory, Menlo Park, California 94025, United States
[#]Department of Photon Science, SLAC National Accelerator Laboratory, Menlo Park, California 94025, United States

Supporting Information

ABSTRACT: The solubility of Ag NPs can affect their toxicity and persistence in the environment. We measured the solubility of organic-coated silver nanoparticles (Ag NPs) having particle diameters ranging from 5 to 80 nm that were synthesized using various methods, and with different organic polymer coatings including poly(vinylpyrrolidone) and gum arabic. The size and morphology of Ag NPs were characterized by transmission electron microscopy (TEM). X-ray absorption fine structure (XAFS) spectroscopy and synchrotron-based total X-ray scattering and pair distribution function (PDF) analysis were used to determine the local structure around Ag and evaluate changes in crystal lattice parameters and structure as a function of NP size. Ag NP solubility dispersed in 1 mM $NaHCO_3$ at pH 8 was found to be well correlated with particle size based on the distribution of measured TEM sizes as predicted by the modified Kelvin equation. Solubility of Ag NPs was not affected by the synthesis method and coating as much as by their size. Based on the modified Kelvin equation, the surface tension of Ag NPs was found to be ~1 J/m^2, which is expected for bulk fcc (face centered cubic) silver. Analysis of XAFS, X-ray scattering, and PDFs confirm that the lattice parameter, *a*, of the fcc crystal structure of Ag NPs did not change with particle size for Ag NPs as small as 6 nm, indicating the absence of lattice strain. These results are consistent with the finding that Ag NP solubility can be estimated based on TEM-derived particle size using the modified Kelvin equation for particles in the size range of 5−40 nm in diameter.

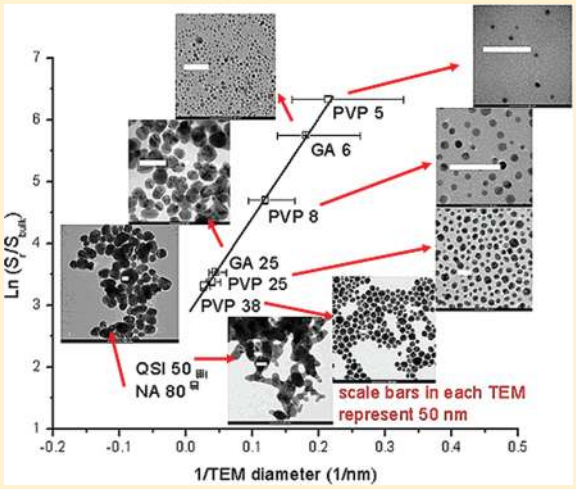

INTRODUCTION

Silver nanoparticles (Ag NPs) are receiving a great deal of attention in the scientific and regulatory communities because of their use in commercial products and release to the environment.[1,2] Silver release to the environment is both an old problem and an emerging challenge.[3] In the United States, colloidal silver has been used as a biocide since 1954.[4] In addition, great quantities of silver releases occurred from photographic film processing since the early 1800s.[5] Silver NPs are reportedly being incorporated into consumer products at a faster rate than any other nanomaterial.[6,7] The properties of Ag NPs that control their spatial and temporal distribution in the environment after release are key to understanding the environmental implications of their release.[8]

Dissolution of Ag NPs (ion release) has been investigated not only because of wide use in commercial products, but also because of the toxicity of silver ions and some other dissolved silver species dissociated from Ag NPs. Toxicity to bacteria,[9] algae,[10] biofilms,[11] aquatic species,[12] and human cells[13] from both Ag NPs and dissolved silver released from them has been demonstrated. In these studies the toxicity of Ag ions released from the Ag NPs is undisputed, highlighting the importance of determining the NP properties affecting their dissolution.

There are many reported methods for synthesizing Ag NPs of varying size, shape, and surface coating.[14,15] The physical properties, synthesis methods, aggregation state, and organic coatings are all believed to affect the dissolution and persistence of engineered nanomaterials such as Ag NPs.[8] The dissolution of Ag NPs of varying size, and with different surface coatings

Received: May 17, 2011
Revised: December 1, 2011
Accepted: December 5, 2011
Published: December 5, 2011

have been reported.[7,9,10,16−24] However differences in experimental conditions, for example pH, dissolved oxygen concentration, buffer type, and supported (in a matrix, e.g. membrane) vs unsupported particles (dispersed in solution) make it difficult to identify which NP and solution properties are controlling Ag NPs dissolution.

The dependence of properties (e.g., reactivity, electrochemical, and optical properties) of engineered nanomaterials on particle size is well recognized.[25−27] For metals and metal oxides, very small particles (<∼10−15 nm in diameter) can have higher surface energy and reactivity compared to larger particles of the same material (e.g., ref 27). The presence of novel properties of nanomaterials compared to bulk materials will depend on whether or not the properties of the particles change with size (e.g., surface tension and strain).[28]

Solubility, an equilibrium property of a material, is a function of particle size and can be described using established thermodynamic relationships. The Kelvin equation (Supporting Information (SI) eq S1) relates the vapor pressure of a liquid droplet to its curvature, which is a function of the droplet size. A modified form of the Kelvin equation (Ostwald-Freundlich relation) is used to relate particle solubility to its radius (eq 1).

$$S_r = S_{\text{bulk}} \times \exp(2\gamma V_m/RT \times r) \quad (1)$$

In eq 1 S_r is the solubility of Ag NPs with radius r, S_{bulk} is the solubility of silver with a flat surface, γ is the surface tension of the particle (J/m^2), V_m is the molar volume of the particle (m^3/mol), R is the gas constant, and T is the temperature (K). Although the applicability of Kelvin's theory to particle-fluid interfaces has been debated, its applicability has been repeatedly verified experimentally.[29−32] The effect of particle radius on NP solubility can be calculated if surface tension is not a function of particle size.[33]

Complications arise in applications of the Ostwald-Freundlich equation for very small particles (<several nanometers in diameter), where surface stress (f), which is the reversible work per unit area required to elastically stretch a surface, can also affect the surface energy of the NPs (eq 2);[34] in other words, there might be strain on the particle.

$$f = \gamma + \partial\gamma/\partial\varepsilon \quad (2)$$

In eq 2 f is surface stress (J/m^2) and ε is the strain tensor (dimensionless). For a liquid, the second term in eq 2 is zero, and surface stress is equal to surface tension, γ. However for very small particles with a large surface to volume ratio, the second term is usually not zero due to lattice contraction or expansion caused by surface stress. Lattice contraction or expansion is also a function of NP radius (eq 3).

$$\Delta a = -2a\kappa f/3r \quad (3)$$

In eq 3 Δa is the relative change of the lattice constant of the nanoparticle, a is the lattice constant of bulk silver, and $\kappa = 9.93\times 10^{-12}$ m^2/N, which is the bulk compressibility of silver.[35] The presence or absence of strain in Ag NPs will depend on lattice contraction or expansion. The Ostwald-Freundlich equation will only apply to solids when the second term of eq 2 is near zero, that is, in the absence of surface strain.[35] Surface tension, lattice contraction, and surface stress of Ag NPs have been studied. However, published estimates of surface tension and surface stress are contradictory.[35]

The Ostwald-Freundlich equation has frequently been invoked to explain the increased solubility of small particles compared to larger ones of the same composition,[33] however, few studies provide experimental data to support this theoretical prediction.[33] There are also few studies on the stability and solubility of very small particles, that is, those less than ca. 10 nm[36] where the effect of NP size on solubility may be observed. Here, we couple observations of nanoparticle behavior in aqueous suspensions along with molecular level investigations of the NP structure to determine how the nanoscale features of the particles, as well as the presence of some commonly used organic polymeric coatings, affects their macroscopic behavior (solubility). The main objective of this study was to determine the extent to which synthesis method, coating type, and nanoparticle size affect Ag NPs solubility in the presence of dissolved oxygen (DO). A second objective was to determine if surface stress was modified in small Ag NPs sufficiently to affect their solubility, and at what nanoparticle size these effects begin to manifest themselves. The structural properties and solubility of Ag NPs synthesized by different methods and with different sizes and polymer coatings were measured. The Ostwald-Freundlich equation was used to correlate TEM size and solubility of Ag NPs. Extended X-ray absorption fine structure (EXAFS) spectroscopy and synchrotron-based X-ray scattering measurements (X-ray diffraction (XRD) and pair distribution function (PDF) analysis) were used to characterize the crystal structure of the Ag NPs.

MATERIALS AND METHODS

Silver nitrate, sodium borohydride, and sodium bicarbonate were purchased from Sigma-Aldrich. Sodium citrate, sodium bicarbonate, gum arabic, poly(vinylpyrrolidone) (PVP, MW 55 000 g/mol), and ethylene glycol were purchased from Fisher Scientific. Gum arabic is a heterogeneous organic macromolecule consisting of a mixture of gum (90%) and glycoprotein (10%). We assume that the MW of gum arabic is approximately 250 000 g/mol.[37] All reagents were used as received without further purification. Ultrapure water (Millipore, 18.2 MΩ·cm) was used to prepare all solutions. Eight separate samples of Ag NPs with different sizes, coatings, and synthesis methods were synthesized or acquired from commercial sources. Gum arabic-stabilized Ag NPs with TEM diameters of 6 nm (Ag GA 6) and 25 nm (Ag GA 25), and PVP-stabilized Ag NPs with TEM diameters of 5 nm (Ag PVP 5), 8 nm (Ag PVP 8), 25 nm (Ag PVP 25), and 38 nm (Ag PVP 38) were synthesized as previously described.[38−40] Details of the synthesis procedure are provided in SI. For lab synthesized Ag NPs, the coatings were shown to be strongly and irreversibly adsorbed on the Ag NPs surface.[41,42] In this study, thermal gravimetric analysis indicated that the organic coating was still present after washing at mg/m^2 levels: 2.8−8.4 mg/m^2 for PVP, and 5.4−17 mg/m^2 for GA coated Ag NPs.[43] As an example, a high resolution TEM image and X-ray Photoelectron Spectroscopy (XPS) spectrum of washed Ag PVP 25 (SI Figure S1) show that the PVP remains after washing. The commercial Ag NPs we characterized include uncoated silver nanoparticles of 50 nm TEM diameter obtained from Quantum Sphere Inc. (Santa Ana, CA) (Ag QSI) and PVP-stabilized Ag NPs with TEM diameters of about 80 nm obtained from Nanostructured & Amorphous Materials Inc. (Houston, TX). Contrary to the lab-synthesized Ag NPs, both commercial Ag NPs were in the form of powders and were dispersed in buffer solution using ultra sonication.

Ag NP Characterization. All of the characterizations were performed on particles that had been washed and redispersed in aqueous 1 mM $NaHCO_3$ solution without PVP or GA in

excess. The sizes of the Ag NPs synthesized were determined using dynamic light scattering (DLS) and TEM imaging. DLS measurements were made using an ALV/CGS-3 compact goniometer system equipped with a 22 mW HeNe Laser (λ = 632.8 nm) at a scattering angle of 90°. TEM images were taken using an FEI Tecnai G2 twin transmission electron microscope at an accelerating voltage of 160 kV. The TEM samples were mounted on Carbon Type A Formvar-coated copper grids from Ted Pella. Samples were prepared by placing one drop of NP suspension on the grid and allowing it to air-dry. TEM size distribution was derived from more than 100 particles of each Ag NP type.

X-ray absorption fine structure (XAFS) spectroscopy and synchrotron-based X-ray diffraction (XRD) with Pair Distribution Function (PDF) analysis were used to assess structural differences among the Ag NPs as a function of size. Both XAFS and XRD samples were washed, redispersed in 1 mM $NaHCO_3$, and then freeze-dried. For XAFS analysis, samples were pelleted after diluting with glucose powder to achieve an optimized absorption edge jump ($\Delta\mu$) of 1. XAFS measurements were conducted at the Stanford synchrotron radiation lightsource (SSRL) on beamline 4−1 to determine if the local structure of the Ag NPs changed as a function of Ag NP size. Ag K-edge (25514 eV) XAFS spectra were collected at room temperature in transmission mode. Data were analyzed using SixPACK software, version 0.60.[44] XAFS scans were energy calibrated using the first derivative (25514 eV) of a metallic Ag calibration standard, background subtracted with E_0 defined as 25514 eV, converted to frequency (k) space, and weighted by k^3. X-ray total scattering data for XRD and PDF analyses were collected at beamline 11-ID-B at the Advanced Photon Source (APS, Argonne National Laboratory), using a Perkin-Elmer amorphous silicon detector. Samples were first mounted in 1 mm Kapton capillaries and were characterized both at λ = 0.2128 Å, (approximately 58 keV) for phase identification by XRD and λ = 0.1370 Å, (approximately 90 keV) for PDF analysis. Images were integrated into intensity vs 2θ plots using Fit2D.[45] The PDFs (or $G(r)$) for all samples were calculated from the Fourier transforms of the reduced structure functions ($f(Q)$) truncated at 28 ± 0.5 $Å^{-1}$ using PDFgetX2.[46] Fitting of the experimental PDFs was performed using the PDFfit2 engine software DiffPy.[47] All PDFs were fit using the known structure of metallic silver (ICSD-64706). Additional details about PDF extractions and fitting are available elsewhere.[48] XRD-based crystallite sizes were determined using the Scherrer line broadening equation on the (111) reflection.[49]

Ag NP Solubility. The solubilities of Ag NPs of different sizes were measured by quantifying dissolved silver in solution with a known initial mass of Ag NPs (typically 5 mg/L) in air saturated (8.6 mg/L DO) 1 mM $NaHCO_3$ solution at pH 8. Prior to the dissolution studies, the Ag NPs were washed two times using DI water to remove excess silver ions and organic coatings resulting from synthesis or during storage. After ultracentrifugation, the supernatant was carefully decanted and an equal volume of deoxygenated DI water (purged with ultrapure N_2 for 30 min) was added. Then the solution was sonicated in an ice-bath (Branson Model 250) with a micro tip at output level 3 (10 W) for 2 min to resuspend the particles. The suspension was agitated for 1 h on an end-over-end rotator at 30 rpm in the dark. This process was repeated once more to remove silver ions in solution prior to dissolution studies.

To determine the solubility of Ag NPs, washed stock solutions (concentration ranging from 20 to 1000 mg/L) were diluted into 120 mL serum bottles to provide the desired initial Ag NPs concentrations (~5 mg/L) in air-saturated 1 mM $NaHCO_3$ at pH 8. Control reactors were acid digested immediately after washing to confirm the total initial silver concentration (C_0) for each Ag NP type (SI Table S1). The serum bottles were sealed with air in the headspace and agitated on the end-overend rotator at 30 rpm in the dark at room temperature (20 °C). Reactors were sampled at time intervals over three months, to determine the dissolved Ag concentration. At each time point, 10 mL of solution was removed for analysis. Particles were separated either by ultra centrifugation or filtration depending on the size as described next. The dissolved fraction (C/C_0) was then determined and reported as the average and standard deviation of duplicate measurements.

Based on preliminary data, ultracentrifugation was sufficient to remove the larger nanoparticles evaluated here (diameters >26 nm). The particle suspension was ultracentrifuged (Beckman with a SW 55 Ti rotor) at 32 000 rpm (84 353g) for 1 h. This speed was chosen because no Ag NPs were detected by UV-vis spectroscopy in the supernatant after centrifugation. For smaller particles (diameters <26 nm), ultra filtration was used to separate dissolved silver from the Ag NPs. Particles were removed using Amicon ultra centrifugal filters (NMWL 3K Da) at 6000g for 20 min. The 3K Da nominal weight cutoff was sufficient to separate Ag NPs from Ag ions. In control studies it was demonstrated that silver ions (added as $AgNO_3$ at 0.1 to 1 mg/L) were 100% recovered, indicating that losses of Ag ions to the filters were negligible.

Acid Digestion and Ag Detection Using Graphite Furnace Atomic Absorption (GFAA). In all cases (i.e., for either total Ag or Ag ion measurements), 9 mL of concentrated nitric acid was added to 1 mL of sample. Samples were digested overnight in the dark before GFAA measurements. The working range of the instrument is 0.001−0.1 mg/L. The standard curve was made by dilution of an atomic absorption silver standard (1000 mg/L). Nitric acid (5% by vol) was maintained at a constant level for all samples and standards to eliminate matrix effects.

RESULTS AND DISCUSSION

Characterization of Ag NPs. Particle sizes determined by TEM and XRD, and hydrodynamic diameters (D_h) determined by DLS for the Ag NPs in this study are summarized in Table 1. All Ag NPs were approximately spherical based on TEM images (Figure 1 and SI S2). All NPs were crystalline based on XRD results (SI Figure S4), despite the different synthesis conditions and coatings used. Figure 1 shows TEM images of Ag GA 6, Ag GA 25, and Ag PVP 38 NPs; TEM images of the other Ag NPs examined in this study are in SI Figure S2.

Ag PVP 38 showed multitwinned icosahedral particles (SI Figure S2). This type of twinning of Ag NPs has been reported previously.[50,51] In contrast, the smallest particles, Ag GA 6, were not twinned. Crystal twinning can change crystal structure and surface energy, thereby affecting the solubility. For example, the defects inherently present in the twinned structure provide active sites for oxidative dissolution.[52] The average TEM diameters ranged from 4.7 to 80 nm, which covers the wide range of sizes seen in consumer products and used in toxicity, ecological, and fate/transformation studies.[10,19,20,28]

X-ray diffraction data for six of the Ag NP samples examined in this study are consistent with the fcc structure of bulk metallic silver (ICSD-64706) (SI Figure S4). There was no evidence in the diffraction patterns for other crystalline phases.

Table 1. TEM/XRD/DLS Sizes, And Measured Solubility of Ag NPs[a]

Ag NPs	TEM diameters (nm)	XRD diameters (nm)	D_h (nm)	dissolution C/C_0 (%)
Ag GA 6	5.5 ± 1.7	6.0	99.9 ± 1.1	51.0 ± 0.3
Ag GA 25	22.8 ± 6.0	13.2	126.8 ± 2.1	5.8 ± 0.1
Ag PVP 5	4.7 ± 1.6	NA	155.7 ± 0.6	62.9 ± 1.6
Ag PVP 8	8.4 ± 2.3	NA	121.0 ± 1.8	14.5 ± 0.6
Ag PVP 25	26.3 ± 6.9	15.2	83.5 ± 1.9	6 ± 0.1
Ag PVP 38	38.2 ± 9.9	15.9	61.6 ± 0.9	4.1 ± 0.23
Ag QSI 50	50.0 ± 15	13.9	198.3 ± 2.0	0.99 ± 0.01
Ag NA 80	76.6 ± 20.7	30.4	89.1 ± 1.5	0.98 ± 0.001

[a] D_h indicates hydrodynamic diameter measured from DLS based on an intensity average in 1 mM $NaHCO_3$ (Table 1). NA indicates not available. The uncertainties shown here are ± one standard deviation. Estimated errors for TEM-derived diameters were based on the measurement of more than 100 particles; for DLS they were calculated from 3 measurements; and for dissolved percentage they were calculated from duplicate reactors.

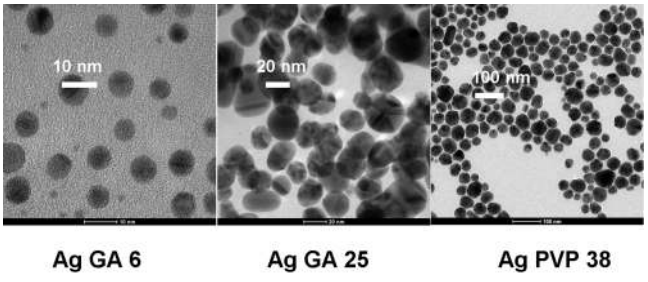

Figure 1. TEM images of Ag GA 6, Ag GA 25, and Ag PVP 38 NPs. Twinning is apparent in the Ag GA 25 and Ag PVP 38 NPs but not in the Ag GA 6 NPs.

Differences in peak broadening are in part related to particle sizes. XRD-derived nanoparticle diameters, determined from peak width at half-maximum using the Scherrer line broadening equation on the first diffraction peak (111), are provided in Table 1. XRD-derived sizes of the smallest particles are similar to their TEM sizes, but XRD sizes are consistently smaller than the TEM sizes for the samples with the larger particles. This is because XRD measures the size of coherent diffraction domains in Ag NPs, which is either equal to the particle diameter for single-crystal particles or smaller than the particle diameter in the case of twinned particles, which have more than one diffraction domain. The nanoparticle sizes determined from DLS are consistently larger than those determined by TEM (Table 1). The larger size determined by DLS compared to TEM is likely a result of both the presence of the coatings which decrease the diffusivity of the particles, giving them a larger hydrodynamic diameter, and from aggregation.

Solubility of Ag NPs of Different Sizes, Coatings, and Synthesis Method. The measured extent of dissolution of the Ag NPs studied here ranged from 1% for the larger particles to up to 60% for the smallest particles. The duration of solubility measurements was two months for smaller particles (Ag PVP 5, Ag PVP 8, and Ag GA 6) and three months for larger particles (Ag NA 80, Ag QSI, Ag PVP 25, Ag PVP 38, and Ag GA 25). Dissolution experiments were stopped only after no significant changes in dissolved Ag concentrations were observed. To our knowledge, the only longer duration studies of Ag NP solubility was by Kittler et al.[18] They measured the dissolution of citrate-coated Ag NPs for 104 days and found that the extent of dissolution of the largest particles (Ag Citrate NP with 50 ± 20 nm TEM size) did not change significantly after 62 days. Based on this observation, we believe that our solubility measurements were at or near true equilibrium.

The solubilities of Ag NPs in the present study increased with decreasing NP size (Figure 2 and Table 1). In the absence

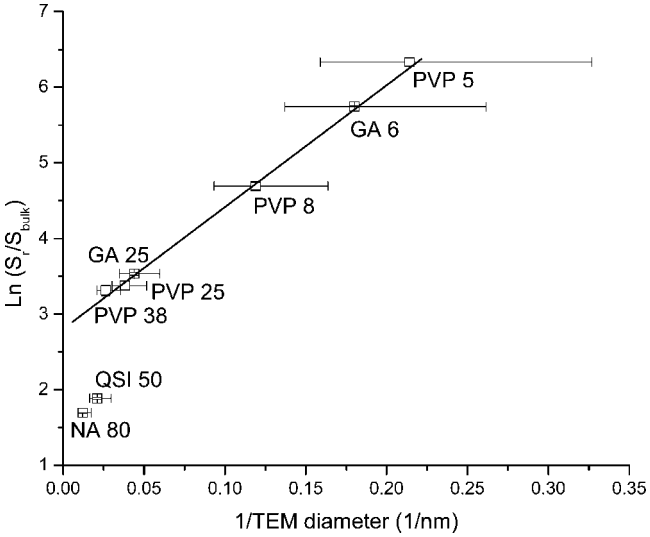

Figure 2. Correlation between Ln S_r/S_{bulk} and 1/TEM diameter of 9 Ag NPs measured in this study, R^2 = 0.993. *y*-axis error bars indicates ± one standard deviation. The two particles equal or larger than 50 nm were not included in the fitting since they both were highly aggregated due to the fact that they had been dried and then redispersed in water and may therefore act more as much larger particles. It is also possible that they may have a Ag_2S shell resulting from exposure to air, thereby limiting dissolution.

of any effects due to NP size or strain, one would expect constant release of Ag^+ species per surface area unit ((Ag^+)/SA) irrespective of particle size (slope = 0 in SI Figure S3), assuming that surface area is reasonably represented by that of a sphere having the measured TEM diameter. A constant release of Ag^+ ion per unit surface area was not observed for the Ag NPs studied here. (SI Figure S3) (The trend line has a positive slope). This indicates that surface area alone did not explain the dissolution of Ag NPs.

A plot of log solubility versus 1/TEM diameter is shown in Figure 2. The good fit of the data by the Ostwald-Freundlich equation indicates that solubility is impacted by the size of the Ag NPs evaluated here. The correlation of log solubility with 1/XRD diameter or 1/DLS diameter is poorer than that of log solubility with 1/TEM diameter (SI Figure S5). This finding suggests that the solubility of Ag NPs may be predicted from their TEM diameter for the coating types and synthesis methods used here, and that it is not affected the limited aggregation observed here (DLS size). It should be noted that this suggestion is for dilute suspensions of Ag NPs at pH 8, where the availability of dissolved oxygen does not limit dissolution. It should also be noted that even though the organic coatings did not affect solubility, they may affect the kinetics of dissolution as has been previously reported.[18,22]

The surface tension of Ag NPs can be determined from the slope of the fit of Ln (S_r/S_{bulk}) vs 1/TEM diameter in Figure 2 using eq 1 (slope = $4\gamma V_m/RT$) and from S_{bulk} = 0.009 mg/L

dx.doi.org/10.1021/es201686j | Environ. Sci. Technol. 2012, 46, 752–759

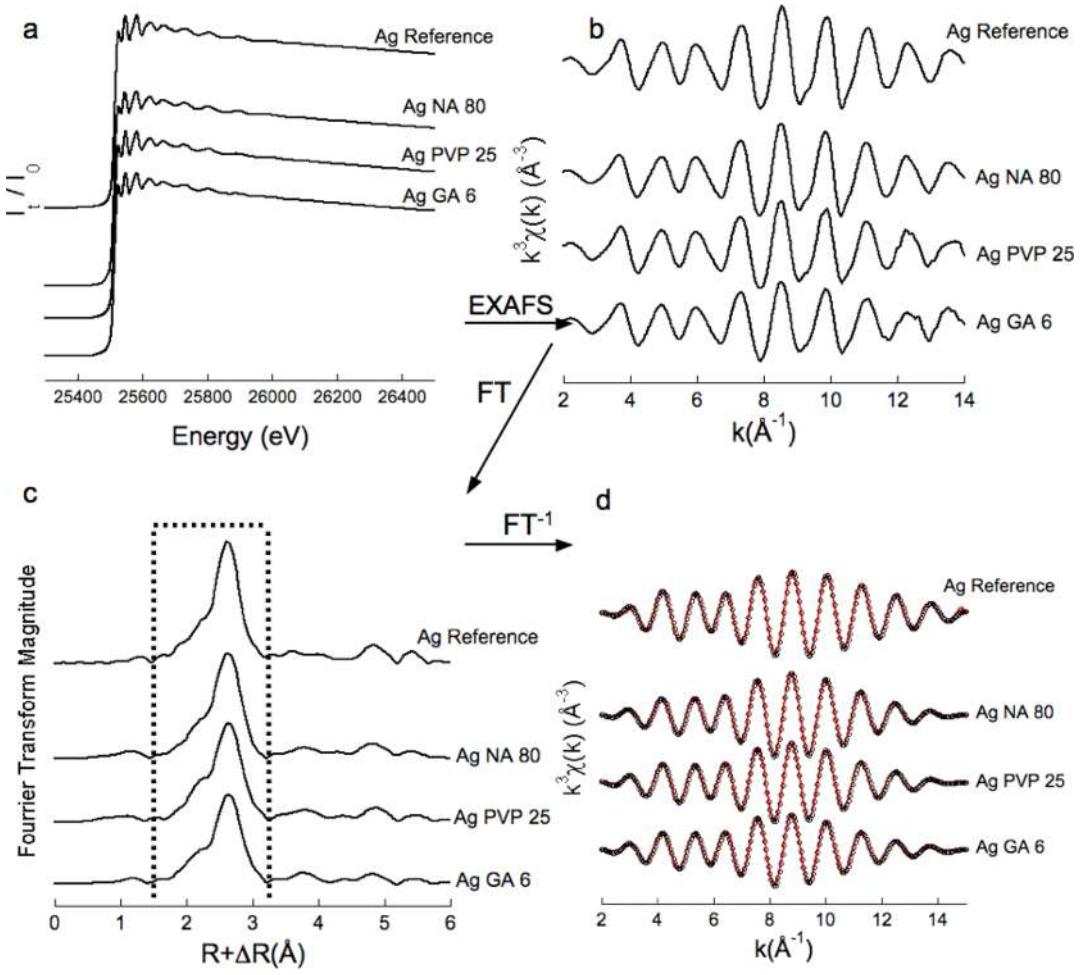

Figure 3. (a) EXAFS spectra for Ag GA 6, Ag PVP 25, and Ag NA 80. (b) Extracted EXAFS oscillations from (a). (c) Fourier transforms of the EXAFS spectra. (d) Back-Fourier transform spectra of the peak (1.5 Å < R < 3.2 Å) shown in (c). Experimental data (circles) and fits (red lines). The EXAFS parameters resulting from the fitting are presented in SI Table S3.

(pH 8), which is measured from a silver plate under the same conditions as the Ag NPs. Using the slope of the fit line (16.55 nm) and assuming V_m = 0.02 nm^3/atom (calculated from the density of bulk silver of 10.5 g/cm^3), we calculated the surface tension of the Ag NPs to be 1 J/m^2. This value is similar to that expected for bulk silver (1.07−1.54 J/m^2).[53] This measured surface tension is consistent with estimates based on the size dependence of the cohesive energy of Ag NPs[54] (1.25 J/m^2), from density functional theory (1.0−2.2 J/m^2),[35] and from modeled evaporation data using the modified Kelvin eq (1.13 J/m^2).[55] The good linear fit of the solubility data to eq 1 also suggests that there was no change in surface tension with decreasing NP size. This would only be true if the Ag NPs studied here are not strained, regardless of their size.

Crystal Structure of Ag NPs. To confirm the absence of strain in the Ag NPs, the average Ag−Ag (first-neighbor) distances and lattice parameters for selected Ag NPs were determined using EXAFS and PDF analyses (Figures 3 and 4). The Fourier transforms of $k^3\chi(k)$ for the three Ag NPs having TEM diameters of 80 nm (Ag NA 80), 26.3 nm (Ag PVP 25), and 5.5 nm (Ag PVP 5) are shown in Figure 3c. The Ag−Ag distances and nearest-neighbor coordination numbers were obtained by fitting the back Fourier transforms (Figure 3d) of the first peak in the Fourier transforms (1.5−3.2 Å R range, Figure 3c), which resulted in average Ag−Ag distances of 2.865 ± 0.002 Å and 10.9 ± 2 first-neighbor Ag atoms. These values are consistent with those expected for bulk fcc silver (Ag−Ag (first-neighbor) distance = 2.879 Å and 12 first-neighbor Ag atoms). More importantly, we did not observe differences in Ag−Ag (first-neighbor) distances (i.e., lattice contraction) as particle size varied, which differs from the findings of previous studies. For example, Battaglin et al.[56] reported lattice contraction of Ag NPs in a glass matrix at diameters ranging from 6 to 8 nm, and Montano et al.[57] also reported lattice contractions in Ag NPs isolated in solid argon with a TEM size of 2.5−13 nm. However, these NPs were synthesized or entrapped in a solid matrix rather than in an aqueous dispersion, as was the case for our samples. Our results are consistent with the theoretical study that predicts significant strain only for particle sizes smaller than 5 nm.[35]

Fourier transformation of the normalized total scattering intensities results in the PDF, which gives the probability of finding an atom at a given distance r from another atom.[58] PDFs of the six Ag NPs examined in this study are shown in Figure 4. Peak positions in the PDFs of the Ag NPs of various sizes are very similar up to a radial distance of 20 Å, indicating similar short- (<∼5 Å) and intermediate-range order (i.e., > ∼5 Å) in the different Ag NPs. The calculated lattice parameters based on PDF fitting are 4.073 ± 0.003 Å, which corresponds to Ag−Ag (first-neighbor) distances of 2.879 ± 0.002 Å,

dx.doi.org/10.1021/es201686j | Environ. Sci. Technol. 2012, 46, 752−759

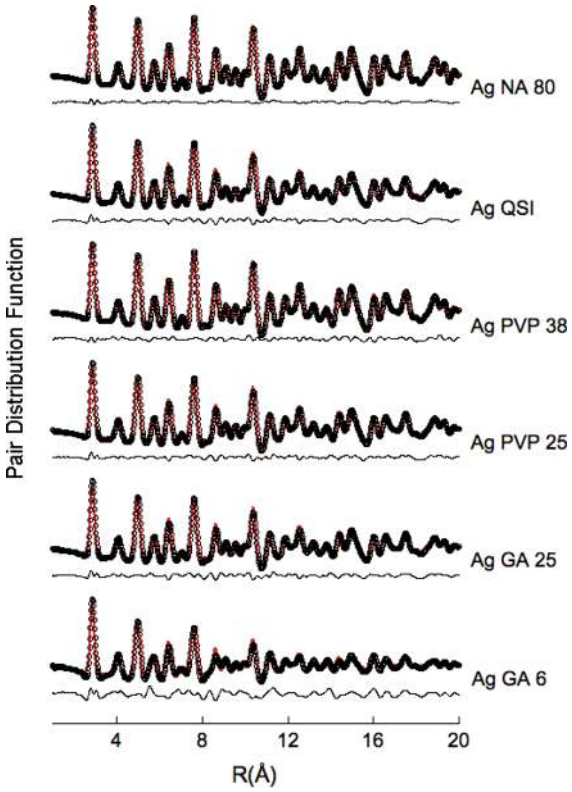

Figure 4. Pair Distribution Functions for Ag GA 6, Ag GA 25, Ag PVP 25, Ag PVP 38, Ag QSI, and Ag NA 80 NPs (circles). Calculated fits are overlain (red) with difference (residual) plots below each experimental and fit PDF.

irrespective of the particle sizes examined (Table 2). This distance is similar to the Ag–Ag distances (2.865 ± 0.002 Å)

Table 2. Nearest Interatomic Distances Determined from Least Square Fits of EXAFS and XRD-PDF Analysis for GA 6, PVP 25, and NA 80 Ag NPs

	Ag–Ag (Å) EXAFS	a (Å) XRD-PDF	Ag–Ag (Å) XRD-PDF
Ag GA 6	2.865 ± 0.002	4.070 ± 0.006	2.878 ± 0.004
Ag PVP 25	2.867 ± 0.002	4.073 ± 0.003	2.880 ± 0.002
Ag NA 80	2.865 ± 0.002	4.073 ± 0.002	2.880 ± 0.002
Ag GA 25	NA	4.073 ± 0.003	2.880 ± 0.002
Ag PVP 38	NA	4.075 ± 0.003	2.881 ± 0.002
Ag QSI	NA	4.071 ± 0.003	2.879 ± 0.002

obtained from XAFS analysis. The good quality of the PDF fits is illustrated by small residuals (Figure 4). However, Ag GA 6 shows a slightly higher residual, and the poorer fit is likely due to local structural defects. Similar behavior as a function of particle size has been observed in a PDF analysis of gold nanoparticles with sizes ranging from 3 to 30 nm.[59] In that study, the relative difficulty of fitting the PDF's of the smallest gold particles was explained by the presence of structural defects and domains inside the nanoparticles. Regardless of structural disorder, the average Ag–Ag bond distances and lattice parameters observed for the samples evaluated here are consistent with bulk fcc Ag (Table 2, SI Figure S6). Size-independent lattice parameters indicate the absence of strain in the Ag NPs studied here. This finding is consistent with our ability to fit the dissolution data (Figure 2) using the Ostwald-Freundlich equation (eq 1) and a surface tension that is independent of Ag NP size.

In summary, our results reveal that smaller Ag NPs have higher solubility and that the increased solubility is related to particle size but not so much to other factors (coating type and synthesis method) examined here. There is no evidence of strain in the Ag NPs examined here and, therefore, no increase in surface tension with decreasing NP size. Based on this finding, the modified Kelvin equation and surface tension determined here (~1 J/m^2) may provide reasonable estimates of Ag NP aqueous solubility as a function of TEM particle diameter for NPs down to 5 nm.

■ ASSOCIATED CONTENT

Supporting Information

Additional data are provided for TEM images and XPS spectrum of washed Ag PVP 25 (Figure S1), TEM images (Figure S2), correlation between solubility and surface area (Figure S3), XRD patterns (Figure S4), correlation between solubility and XRD and DLS size (Figure S5), Ag fcc crystal structure and bond distances (Figure S6). Initial and equilibrium silver concentration and recoveries (Table S1), polydispersity index and specific surface area (Table S2). EXAFS fitting parameters of the back-Fourier transform spectra corresponding to the first atomic shell (Table S3). This material is available free of charge via the Internet at http://pubs.acs.org.

■ AUTHOR INFORMATION

Corresponding Author

*E-mail: glowry@cmu.edu.

■ ACKNOWLEDGMENTS

This material is based upon work supported by the National Science Foundation (NSF and the Environmental Protection Agency (EPA) under NSF Cooperative Agreement EF-0830093, Center for the Environmental Implications of Nanotechnology (CEINT) and EPA (R833326). Portions of this research were carried out at the Stanford Synchrotron Radiation Lightsource (SSRL), a national user facility operated by Stanford University on behalf of the U.S. Department of Energy, Office of Basic Energy Sciences and located at the SLAC National Accelerator Laboratory. Use of the Advanced Photon Source, an Office of Science User Facility operated for the U.S. Department of Energy (DOE) Office of Science by Argonne National Laboratory, was supported by the U.S. DOE under Contract No. DE-AC02-06CH11357. We also thank the staff of APS (BL 11-ID-B) and SSRL (BL 4-1).

■ REFERENCES

(1) Faunce, T.; Watal, A. Nanosilver and global public health: international regulatory issues. *Nanomedicine* **2010**, *5* (4), 617–632.

(2) Benn, T. M.; Westerhoff, P. Nanoparticle silver released into water from commercially available sock fabrics. *Environ. Sci. Technol.* **2008**, *42* (11), 4133–4139.

(3) Luoma, S. N., Silver nanotechnologies and the environment: Old problems or new challenges? Project on emerging nanotechnology [online], September 2008. http://www.nanotechproject.org/process/assets/files/7036/nano_pen_15_final.pdf.

(4) Bernd Nowack, H. F. K.; Height, Murray 120 Years of nanosilver history: Implications for policy makers. *Environ. Sci. Technol.* **2011**, *45* (4), 1177–1183.

(5) Luoma, S. N.; Ho, Y. B.; Bryan, G. W. Fate, bioavailability and toxicity of silver in estuarine environments. *Mar. Pollut. Bull.* **1995**, *31* (1−3), 44−54.
(6) Tolaymat, T. M.; El Badawy, A. M.; Genaidy, A.; Scheckel, K. G.; Luxton, T. P.; Suidan, M. An evidence-based environmental perspective of manufactured silver nanoparticle in syntheses and applications: A systematic review and critical appraisal of peer-reviewed scientific papers. *Sci. Total Environ.* **2010**, *408* (5), 999−1006.
(7) Liu, J. Y.; Hurt, R. H. Ion release kinetics and particle persistence in aqueous nano-silver colloids. *Environ. Sci. Technol.* **2010**, *44* (6), 2169−2175.
(8) Wiesner, M. R.; Lowry, G. V.; Jones, K. L.; Hochella, M. F.; Di Giulio, R. T.; Casman, E.; Bernhardt, E. S. Decreasing uncertainties in assessing environmental exposure, risk, and ecological implications of nanomaterials. *Environ. Sci. Technol.* **2009**, *43* (17), 6458−6462.
(9) Suresh, A. K.; Pelletier, D. A.; Wang, W.; Moon, J. W.; Gu, B. H.; Mortensen, N. P.; Allison, D. P.; Joy, D. C.; Phelps, T. J.; Doktycz, M. J. Silver nanocrystallites: biofabrication using *Shewanella oneidensis*, and an evaluation of their comparative toxicity on gram-negative and gram-positive bacteria. *Environ. Sci. Technol.* **2010**, *44* (13), 5210−5215.
(10) Navarro, E.; Piccapietra, F.; Wagner, B.; Marconi, F.; Kaegi, R.; Odzak, N.; Sigg, L.; Behra, R. Toxicity of silver nanoparticles to *Chlamydomonas reinhardtii*. *Environ. Sci. Technol.* **2008**, *42* (23), 8959−8964.
(11) Fabrega, J.; Renshaw, J. C.; Lead, J. R. Interactions of silver nanoparticles with *Pseudomonas putida* biofilms. *Environ. Sci. Technol.* **2009**, *43* (23), 9004−9009.
(12) Allen, H. J.; Impellitteri, C. A.; Macke, D. A.; Heckman, J. L.; Poynton, H. C.; Lazorchak, J. M.; Govindaswamy, S.; Roose, D. L.; Nadagouda, M. N. Effects from filtration, capping agents, and presence/absence of food on the toxicity of silver nanoparticles to *Daphnia magna*. *Environ. Toxicol. Chem.* **2010**, *29* (12), 2742−2750.
(13) Wise, S. S.; Mason, M. D.; Holmes, A. H.; Savery, L. C.; Li, C. T.; Goodale, B. C.; Shaffiey, F.; Wise, J. P.; Craig, G.; Walter, R. B.; Payne, R.; Kerr, I. A. R.; Spaulding, M.; Wise, J. P. Cytotoxicity and genotoxicity of silver nanoparticles in human and marine cell lines. *Environ. Mol. Mutagen.* **2007**, *48* (7), 606−606.
(14) Sun, Y. G.; Xia, Y. N. Shape-controlled synthesis of gold and silver nanoparticles. *Science* **2002**, *298* (5601), 2176−2179.
(15) Chen, B.; Jiao, X. L.; Chen, D. R. Size-controlled and size-designed synthesis of nano/submicrometer Ag particles. *Cryst. Growth Des.* **2010**, *10* (8), 3378−3386.
(16) Damm, C.; Munstedt, H. Kinetic aspects of the silver ion release from antimicrobial polyamide/silver nanocomposites. *Appl. Phys. A: Mater. Sci. Process.* **2008**, *91* (3), 479−486.
(17) Jin, X.; Li, M. H.; Wang, J. W.; Marambio-Jones, C.; Peng, F. B.; Huang, X. F.; Damoiseaux, R.; Hoek, E. M. V. High-throughput screening of silver nanoparticle stability and bacterial inactivation in aquatic media: Influence of specific ions. *Environ. Sci. Technol.* **2010**, *44* (19), 7321−7328.
(18) Kittler, S.; Greulich, C.; Diendorf, J.; Koller, M.; Epple, M. Toxicity of silver nanoparticles increases during storage because of slow dissolution under release of silver ions. *Chem. Mater.* **2010**, *22* (16), 4548−4554.
(19) Kennedy, A. J.; Hull, M. S.; Bednar, A. J.; Goss, J. D.; Gunter, J. C.; Bouldin, J. L.; Vikesland, P. J.; Steevens, J. A. Fractionating nanosilver: Importance for determining toxicity to aquatic test organisms. *Environ. Sci. Technol.* **2010**, *44* (24), 9571−9577.
(20) Sotiriou, G. A.; Pratsinis, S. E. Antibacterial activity of nanosilver ions and particles. *Environ. Sci. Technol.* **2010**, *44* (14), 5649−5654.
(21) Liu, J. Y.; Sonshine, D. A.; Shervani, S.; Hurt, R. H. Controlled release of biologically active silver from nanosilver surfaces. *ACS Nano* **2010**, *4* (11), 6903−6913.
(22) Zhang, W.; Yao, Y.; Sullivan, N.; Chen, Y. S. Modeling the primary size effects of citrate-coated silver nanoparticles on their ion release kinetics. *Environ. Sci. Technol.* **2011**, *45* (10), 4422−4428.
(23) Stebounova, L. V.; Guio, E.; Grassian, V. H. Silver nanoparticles in simulated biological media: A study of aggregation, sedimentation, and dissolution. *J. Nanopart. Res.* **2011**, *13* (1), 233−244.
(24) Li, X. A.; Lenhart, J. J.; Walker, H. W. Dissolution-accompanied aggregation kinetics of silver nanoparticles. *Langmuir* **2010**, *26* (22), 16690−16698.
(25) Ivanova, O. S.; Zamborini, F. P. Size-dependent electrochemical oxidation of silver nanoparticles. *J. Am. Chem. Soc.* **2010**, *132* (1), 70−72.
(26) Yeshchenko, O. A.; Dmitruk, I. M.; Alexeenko, A. A.; Losytskyy, M. Y.; Kotko, A. V.; Pinchuk, A. O. Size-dependent surface-plasmon-enhanced photoluminescence from silver nanoparticles embedded in silica. *Phys. Rev. B* **2009**, *79* (23), 8.
(27) Yang, C. C.; Li, S. Size-dependent phase stability of silver nanocrystals. *J. Phys. Chem. C* **2008**, *112* (42), 16400−16404.
(28) Auffan, M.; Rose, J.; Bottero, J. Y.; Lowry, G. V.; Jolivet, J. P.; Wiesner, M. R. Towards a definition of inorganic nanoparticles from an environmental, health and safety perspective. *Nat. Nanotechnol.* **2009**, *4* (10), 634−641.
(29) Dundon, M. L. The surface energy of several salts. *J. Am. Chem. Soc.* **1923**, *45*, 2658−2666.
(30) Dundon, M. L.; Mark, E. J. The solubility and surface energy of calcium sulphate. *J. Am. Chem. Soc.* **1923**, *45*, 2479−2485.
(31) Brunauer, S.; Hayes, J. C.; Hass, W. E. The heats of hydration of tricalcium silicate and beta-dicalcium silicate. *J. Phys. Chem.* **1954**, *58* (3), 279−285.
(32) Benson, G. C.; Benson, G. W. Surface energies of the alkali halides. *Can. J. Chem.-Rev. Can. Chim.* **1955**, *33* (2), 232−239.
(33) Liu, J.; Aruguete, D. M.; Murayama, M.; Hochella, M. F. Influence of size and aggregation on the reactivity of an environmentally and industrially relevant manomaterial (PbS). *Environ. Sci. Technol.* **2009**, *43* (21), 8178−8183.
(34) Hofmeister, H.; Thiel, S.; Dubiel, M.; Schurig, E. Synthesis of nanosized silver particles in ion-exchanged glass by electron beam irradiation. *Appl. Phys. Lett.* **1997**, *70* (13), 1694−1696.
(35) Medasani, B.; Park, Y. H.; Vasiliev, I. Theoretical study of the surface energy, stress, and lattice contraction of silver nanoparticles. *Phys. Rev. B* **2007**, *75* (23), 6.
(36) Bian, S. W.; Mudunkotuwa, I. A.; Rupasinghe, T.; Grassian, V. H. Aggregation and dissolution of 4 nm ZnO nanoparticles in aqueous environments: Influence of pH, ionic strength, size, and adsorption of humic acid. *Langmuir* **2011**, *27* (10), 6059−6068.
(37) Renard, D.; Lavenant-Gourgeon, L.; Ralet, M. C.; Sanchez, C. Acacia senegal gum: Continuum of molecular species differing by their protein to sugar ratio, molecular weight, and charges. *Biomacromolecules* **2006**, *7* (9), 2637−2649.
(38) Lee, P. C.; Meisel, D. Adsorption and surface-enhanced raman of dyes on silver and gold sols. *J. Phys. Chem.* **1982**, *86* (17), 3391−3395.
(39) Silvert, P. Y.; HerreraUrbina, R.; Duvauchelle, N.; Vijayakrishnan, V.; Elhsissen, K. T. Preparation of colloidal silver dispersions by the polyol process 0.1. Synthesis and characterization. *J. Mater. Chem.* **1996**, *6* (4), 573−577.
(40) Silvert, P. Y.; HerreraUrbina, R.; TekaiaElhsissen, K. Preparation of colloidal silver dispersions by the polyol process 0.2. Mechanism of particle formation. *J. Mater. Chem.* **1997**, *7* (2), 293−299.
(41) Kim, H. J.; Phenrat, T.; Tilton, R. D.; Lowry, G. V. Fe(0) nanoparticles remain mobile in porous media after aging due to slow desorption of polymeric surface modifiers. *Environ. Sci. Technol.* **2009**, *43* (10), 3824−3830.
(42) Munro, C. H.; Smith, W. E.; Garner, M.; Clarkson, J.; White, P. C. Characterization of the surface of a citrate-reduced colloid optimized for use as a substrate for surface-enhanced resonance raman-scattering. *Langmuir* **1995**, *11* (10), 3712−3720.
(43) Song, J. E.; Phenrat, T.; Marinakos, S.; Xiao, Y.; Liu, J.; Wiesner, M. R.; Tilton, R. D.; Lowry, G. V. Hydrophobic interactions increase attachment of gum arabic- and PVP-coated Ag nanoparticles to hydrophobic surfaces. *Environ. Sci. Technol.* **2011**, *45* (14), 5988−5995.

(44) Webb, S. M. SIXpack: a graphical user interface for XAS analysis using IFEFFIT. *Phys. Scr.* **2005**, *T115*, 1011−1014.
(45) Hammersley, A. P.; Svensson, S. O.; Hanfland, M.; Fitch, A. N.; Hausermann, D. Two-dimensional detector software: From real detector to idealised image or two-theta scan. *High Pressure Res.* **1996**, *14* (4−6), 235−248.
(46) Qiu, X.; T. a., J. W.; B., S. J. L. PDFgetX2: A GUI-driven program to obtain the pair distribution function from X-ray powder diffraction data. *J. Appl. Crystallogr.* **2004**, *37*, 678.
(47) Farrow, C. L.; Juhas, P.; Liu, J. W.; Bryndin, D.; Bozin, E. S.; Bloch, J.; Proffen, T.; Billinge, S. J. L. PDFfit2 and PDFgui: computer programs for studying nanostructure in crystals. *J. Phys.-Condes. Matter* **2007**, *19* (33), 7.
(48) Michel, F. M.; Barron, V.; Torrent, J.; Morales, M. P.; Serna, C. J.; Boily, J. F.; Liu, Q. S.; Ambrosini, A.; Cismasu, A. C.; Brown, G. E. Ordered ferrimagnetic form of ferrihydrite reveals links among structure, composition, and magnetism. *Proc. Natl. Acad. Sci. U. S. A.* **2010**, *107* (7), 2787−2792.
(49) Birks, L. S.; Friedman, H. Particle size determination from X-ray line broadening. *J. Appl. Phys.* **1946**, *17* (8), 687−691.
(50) Elechiguerra, J. L.; Reyes-Gasga, J.; Yacaman, M. J. The role of twinning in shape evolution of anisotropic noble metal nanostructures. *J. Mater. Chem.* **2006**, *16* (40), 3906−3919.
(51) Callegari, A.; Tonti, D.; Chergui, M. Photochemically grown silver nanoparticles with wavelength-controlled size and shape. *Nano Lett.* **2003**, *3* (11), 1565−1568.
(52) Wiley, B.; Herricks, T.; Sun, Y. G.; Xia, Y. N. Polyol synthesis of silver nanoparticles: Use of chloride and oxygen to promote the formation of single-crystal, truncated cubes and tetrahedrons (vol 4, pg 1734, 2004). *Nano Lett.* **2004**, *4* (10), 2057−2057.
(53) Fournier, R. Theoretical study of the structure of silver clusters. *J. Chem. Phys.* **2001**, *115* (5), 2165−2177.
(54) Jiang, Q.; Liang, L. H.; Zhao, D. S. Lattice contraction and surface stress of fcc nanocrystals. *J. Phys. Chem. B* **2001**, *105* (27), 6275−6277.
(55) Blackman, M.; Lisgarte., Nd; Skinner, L. M. Surface energy and evaporation rate of spherical particles of radii less than 500 A. *Nature* **1968**, *217* (5135), 1245−&.
(56) Battaglin, G.; Cattaruzza, E.; Gonella, F.; Pollini, R.; D'Acapito, F.; Colonna, S.; Mattei, G.; Maurizio, C.; Mazzoldi, P.; Padovani, S.; Sada, C.; Quaranta, A.; Longo, A. Silver nanocluster formation in ion-exchanged glasses by annealing, ion beam and laser beam irradiation: An EXAFS study. *Nucl. Instrum. Methods Phys. Res. Sect. B-Beam Interact. Mater. Atoms* **2003**, *200*, 185−190.
(57) Montano, P. A.; Schulze, W.; Tesche, B.; Shenoy, G. K.; Morrison, T. I. Extended X-ray-absorption fine-structure study of Ag particles isolated in solid argon. *Phys. Rev. B* **1984**, *30* (2), 672−677.
(58) Proffen, T.; Billinge, S. J. L.; Egami, T.; Louca, D. Structural analysis of complex materials using the atomic pair distribution function—A practical guide. *Z. Kristallogr.* **2003**, *218* (2), 132−143.
(59) Petkov, V.; Peng, Y.; Williams, G.; Huang, B. H.; Tomalia, D.; Ren, Y. Structure of gold nanoparticles suspended in water studied by x-ray diffraction and computer simulations. *Phys. Rev. B* **2005**, *72* (19), 8.